

CME projection effects studied with STEREO/COR and SOHO/LASCO

M. TEMMER, S. PREISS, A.M. VERONIG
*IGAM/Institute of Physics, University of Graz,
Universitätsplatz 5, A-8010 Graz, Austria*

Abstract

Based on a set of eleven CME events we study the impact of projection effects by tracking CME leading edge features in the plane-of-sky (traditional CME tracking) from combined STEREO/SECCHI-SOHO/LASCO observations up to $20R_{\odot}$. Using CME observations from two vantage points and applying triangulation techniques, the source region location of the CME on the solar surface was determined (heliospheric longitude and latitude) in order to correct for projection effects. With this information, the directivity and ‘true’ speed of a CME can be estimated in a simple way. The comparison of the results obtained from the spacecraft pairs SOHO-LASCO/STEREO-A and SOHO-LASCO/STEREO-B allows us to study the reliability of the method. The determined CME source region is generally coincident within $\lesssim 10^{\circ}$.

1 Introduction

Coronal mass ejections (CMEs), clouds of magnetized plasma expelled from the Sun to interplanetary space with velocities up to a few 1000 km s^{-1} , are by far the most violent activity signatures from our Sun. They appear as outward moving structures originating from the solar corona, and are most often observed in photospheric white light scattered by coronal electrons (Thomson scattering; e.g. Gosling et al. 1974). A comprehensive book on CME studies was just recently issued by the International Space Science Institute (Kunow et al. 2007), among others presenting a historical overview (Alexander et al. 2006), an observational review (Hudson et al. 2006), and an overview on current theoretical and modelling efforts (Forbes et al. 2006). Despite the extensive studies which were carried out after their discovery in the 1970’s, our understanding of the physical characteristics of CMEs is still limited. In single coronagraph observations which image CMEs in projection against the plane-of-sky, the 3D structure and evolution is missing (Howard et al. 1985; Hundhausen 1993; Webb & Howard 1994; Sheeley et al. 1999; St. Cyr et al. 2000). Hence, the importance of projection effects, i.e. the 2D plane-of-sky projection of a 3D structure, on the inferred

CME kinematics, is still a matter of debate (Cremades & Bothmer 2004; Ciavarella et al. 2006; Vršnak et al. 2007). Basic observational CME parameters like the angular width, the structure, propagation direction and subsequently derived quantities like velocities and accelerations are biased by projection effects (see e.g. Burkepile et al. 2004; Schwenn et al. 2005). The extent of projection mainly depends on the location of the CME source region on the solar surface with respect to the view of the observer. Therefore, to determine the directivity and ‘true’, i.e. de-projected, velocity of CMEs we need to know the location of their source regions on the Sun. This is of great importance, since in particular fast and Earth-directed CMEs may cause severe geomagnetic disturbances (see, e.g., Webb et al. 2000; Zhang et al. 2003; Michalek et al. 2003; Xue et al. 2005; Bothmer 2006; Webb et al. 2006). The travel time of CMEs from the Sun to their arrival at Earth is strongly dependent on the CME speed (Gopalswamy et al. 2000, 2001; Michalek et al. 2003; Xue et al. 2005) as well as on their interaction with the ambient solar wind flow in the interplanetary space (e.g. Vršnak & Žic 2007, and references therein). A kinematic treatment of CME evolution in the solar wind is assumed to increase the accuracy of forecasting transit times (Gopalswamy et al. 2001; Riley & Crooker 2004; Vršnak et al. 2004).

To correct for projection effects, different geometrical and statistical methods applied to data from the *Solar and Heliospheric Observatory - Large Angle Spectroscopic Coronagraph* (SOHO-LASCO; Brueckner et al. 1995) have been utilized (see Michalek et al. 2007; Vršnak et al. 2007; Howard et al. 2008b; Yashiro et al. 2008), as well as modeling efforts based on different geometrical shapes for the CMEs as observed by LASCO (e.g. Sheeley et al. 1999; Leblanc et al. 2001; Thernisien et al. 2006). Observations from the *Solar Terrestrial Relations Observatory* (STEREO; Kaiser et al. 2008), launched in 2006, provide us with unprecedented opportunities to validate and improve current models. STEREO consists of two identical satellites, positioned ahead (A) and behind (B) the Earth on its orbit around the Sun. Thus, STEREO observes the Sun from two different vantage points (different from that of LASCO aboard SOHO, positioned at L1), which provides us with the first 3D insight of CMEs. Their steadily increasing separation angles from Earth ($\sim 22.5^\circ$ per year) enables us to observe and measure a CME by both STEREO satellites and SOHO-LASCO with varying vantage points. From the kinematics derived from the different instruments, the CME 3D propagation direction and the source region can be determined which in consequence enables us to remove, at least partly, projection effects from the kinematics. Studies based on a small selection of STEREO events by Howard & Tappin (2008), Mierla et al. (2008), and Liewer et al. (2008) have already demonstrated that triangulation methods are effective and quick in determining the 3D evolution and source region positions, in order to obtain de-projected propagation directions and velocities of CMEs (see also Pizzo & Biesecker 2004).

In this paper, we analyze the impact of projection effects on measurements of the CME kinematics by probing the ‘traditional’ CME tracking method. The aim is to study the accuracy and limitations of traditional plane-of-sky measurements, and hence, to improve the interpretation of ‘non 3D’ data. Since

the STEREO 3D mapping ability is restricted in time, future CME observations will be based again on single coronagraphic 2D images. Comparing the plane-of-sky leading edge measurements as gained from STEREO-A (COR1, COR2), STEREO-B (COR1, COR2), and SOHO-LASCO (C2, C3) observations, we calculate from the differences in the measured CME kinematics, the CME’s source region location on the solar surface. With the information of the source region, we can correct for projection and get an estimate of the de-projected CME kinematics and velocities. For our study, we selected eleven well observed CME events which could be tracked to a distance of $\sim 20R_{\odot}$.

2 Method of triangulation

By applying a geometric triangulation method (cf. Figure 1), the longitude and latitude of the CME source region on the solar surface can be derived via observations of the CME from at least two different vantage points. By carefully measuring a common CME feature, identified in all three instruments, in projection against the plane-of-sky (POS), we derive three separate height-time plots from STEREO-A, STEREO-B and LASCO observations. Common features were chosen close to the central part of the leading edge, along the main propagation direction. We tracked conspicuous features of the leading edge, like density variations or prominently shaped structures (cf. arrows in Figures 2–4). Employing the information of the spacecraft separation angle (LASCO-STEREO) and taking the source region location as free parameter, the measured projected distances from LASCO are used to model those distances which would be observed from the STEREO views. Comparing the modeled distances with the distances observed from STEREO, that source region location, which gives the minimum deviation, results in the best estimation of the ‘true’ CME source region location. Observations from two different vantage points are then used to pin-down the position of the source region which is subsequently used to correct for projection effects and to derive the de-projected kinematics and speed of a CME. For our analysis, we take SOHO-LASCO (LASCO) as reference system and the triangulation is carried out separately between two pairs of spacecraft, namely LASCO/STEREO-A (LA) and LASCO/STEREO-B (LB). This allows us to quantify the reliability and accuracy of the method.

The triangulation method is illustrated in Figure 1 and will be described on the example of spacecraft pair LA. For the analysis we assume a radial outward motion of the CME and the spacecraft to be co-planar in the ecliptic plane¹. The spacecraft pair LA observes the leading edge of a CME (red disk) having the ‘true’ distance d from the Sun. The measured CME distances d_{0A} , d_{0L} and measured position angles (PA-A, PA-L), projected against the POS of each spacecraft, which are separated from each other by φ_A , are different. Close to the Sun up to $30 R_{\odot}$ the elongation angles in radians can be directly converted to distance in units of R_{\odot} , and for LASCO $d_{0L} \sim 216R_{\odot}\lambda$, where λ is the elongation

¹Variation for STEREO-A and -B against the ecliptic are in the range of $\pm 0.2^{\circ}$ which we further neglect in our study.

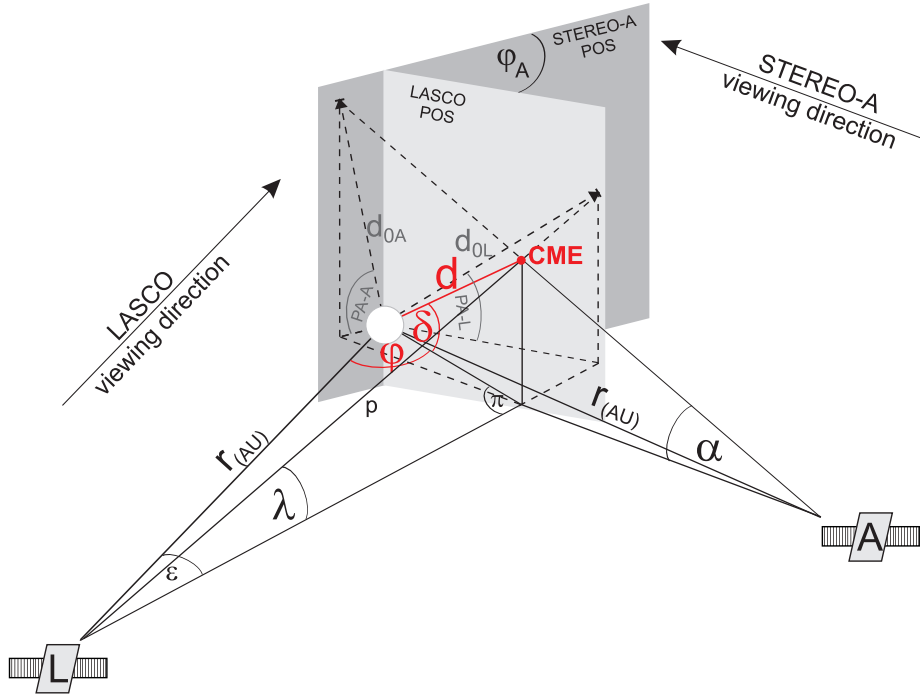


Figure 1: Schematic LASCO and STEREO-A view observing the leading edge of a CME (red disk). The separation angle between the two spacecraft is φ_A . The different plane-of-sky (POS) measurements, d_{0L} , d_{0A} , of the real CME distance d , is shown together with the elongation angles, λ and α , i.e. the angular distances between the spacecraft-CME leading edge projected onto the equatorial plane and spacecraft-CME leading edge. The angles ε and π lie in the equatorial plane. The heliographic longitude and latitude of the CME source region on the solar surface are indicated with φ and δ . PA-A and PA-L are the measured position angles of the CME observed from spacecraft STEREO-A and LASCO.

angle (cf. Howard et al. 2006; Vourlidas & Howard 2006; Howard et al. 2008b). According to this relation, we can model the CME distance by calculating the elongation angles. LASCO serves as reference system and the calculation of the elongation angle α (STEREO-A view) is thus based on d_{0L} . The elongation angle α , and hence the modeled CME distance from STEREO-A view, is then derived in dependence on the position of the spacecraft STEREO-A relative to LASCO, φ_A , and the source region longitude φ and latitude δ . The parameters are calculated using the following formulae (cf. Figure 1):

$$\varepsilon = \arctan\left(\frac{d_{0L}}{r_{AU}}\right), \quad (1)$$

$$\pi = 180 - \varepsilon - \varphi, \quad (2)$$

$$d = \frac{r_{AU}}{\sin \pi} \cdot \sin \varepsilon, \quad (3)$$

$$\delta = \arctan(\tan(\text{PA-A}) \cdot \sin(\varphi \pm \varphi_A)), \quad (4)$$

$$p^2 = d^2 + r_{AU}^2 - 2 \cdot \sin \delta \cdot \cos \delta \cdot \cos(\varphi \pm \varphi_A), \text{ and} \quad (5)$$

$$\alpha = \arccos\left(\frac{r_{AU}^2 + p^2 - d^2}{2 \cdot r_{AU} \cdot \sqrt{p}}\right). \quad (6)$$

Applying an iterative algorithm by varying the source region longitude φ and latitude δ , we find the minimum deviation between modeled (from α) and measured projected distances (d_{0A}) resulting in the best estimation of the source region location of the CME. From the measured projected distances (d_{0A}) we estimate the true, i.e. the de-projected, distance d by inserting the derived longitude φ to Equations 1–3. The minimum difference is obtained by the least square error method. In the same way the best estimation of the source region location from LB observations is derived by comparing the modeled distance from β with the measured distance d_{0B} , using the information of the spacecraft separation angle φ_B and the measured position angle PA-B.

The distances and heliographic coordinates are given with respect to LASCO, i.e. Earth-view of $\varphi = 0$, in Stonyhurst heliographic coordinates (see Thompson 2006). The longitude φ is iteratively varied in the range E0°–E180° and W0°–W180° in steps of 1°. The latitude δ for the calculation of the elongation angles, is varied over a smaller range around a first approximation determined from the measured position angles from the three spacecraft (PA[-A,-B,-L]) of the CME. Note that PA is used here, against usual conventions, for the ranges $-90^\circ < \text{PA-East} < +90^\circ$ and $-90^\circ < \text{PA-West} < +90^\circ$. The relation between observed PA and δ is given in Equation 4 in dependence on the vantage point of the spacecraft φ_A (or φ_B) and the source region longitude φ (see also Howard & Tappin 2008). The range of δ is given from N0°–N90° to S0°–S90°.

3 Results

The data are taken from the *Sun Earth Connection Coronal and Heliospheric Investigation* (SECCHI; Howard et al. 2008a) COR1 and COR2 instruments

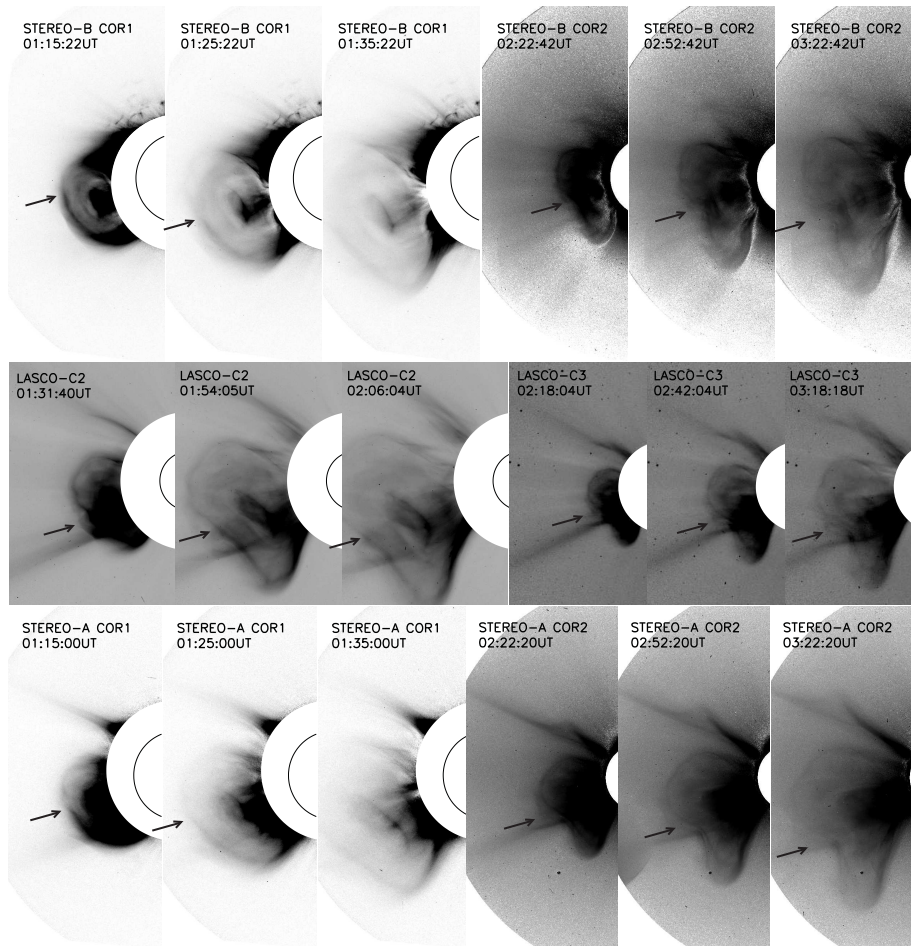


Figure 2: Coronagraph images from December 31, 2007 using a reversed color table (i.e. high intensities appear dark). Top and bottom row: STEREO-B and STEREO-A images from COR1 (total brightness) and COR2 (polarized brightness). The images are prepared by subtracting the monthly background and a pre-event a few hours before the event. Middle row: LASCO C2 and C3 images.

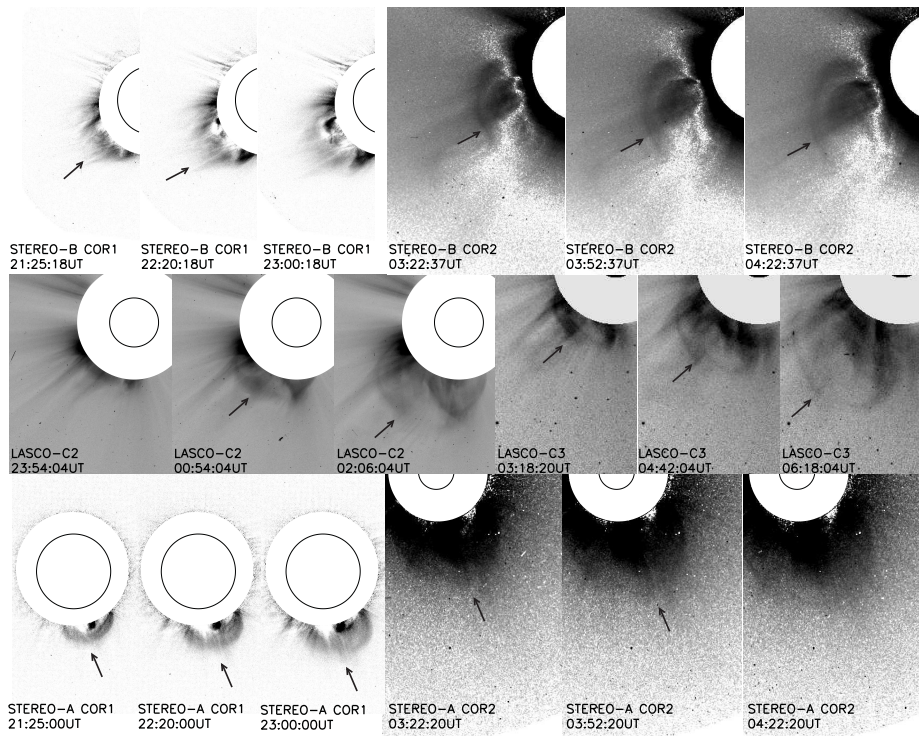


Figure 3: Coronagraph images from January 22, 2008. Images are arranged and prepared in the same way as described in Figure 2.

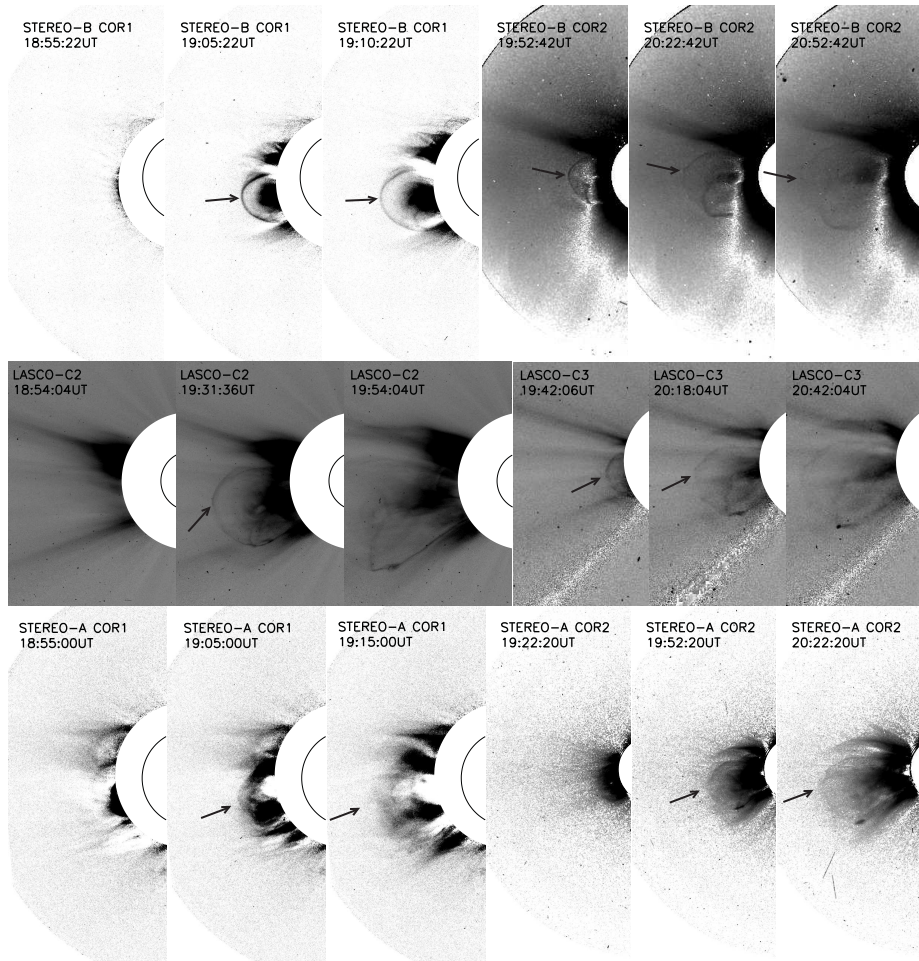


Figure 4: Coronagraph images from March 25, 2008. Images are arranged and prepared in the same way as described in Figure 2.

aboard the *Solar Terrestrial Relations Observatory* STEREO-A and -B spacecraft (Kaiser et al. 2008). COR1 is the inner coronagraph which observes the Sun in white light from 1.4–4 R_{\odot} . From COR1 data the total brightness images were used for our study. COR2 is the outer coronagraph which observes the Sun from 2–15 R_{\odot} . For our study we used polarized brightness COR2 images. From the *Solar and Heliospheric Observatory mission* (SOHO) data are taken from the *Large Angle Spectroscopic Coronagraph* (LASCO; Brueckner et al. 1995) C2 (1.5–6 R_{\odot}) and C3 (3.5–30 R_{\odot}).

In Figures 2–4 processed COR1, COR2 (from STEREO-A and STEREO-B) as well as LASCO C2 and C3 images are shown for three of the events under study. The preparation of the data was done very thoroughly to maximize the contrast in order to identify a common CME feature (density variations, prominently shaped structures as indicated by arrows in Figures 2–4) in all three spacecraft. The level-0 data were properly prepared using SolarSoft routines and all images were rotated to solar north up. To additionally enhance the contrast for STEREO observations, we subtracted a pre-event image a few hours before the event. For nearly all the events this procedure was satisfactory with exception of October 8, 2007 and December 16, 2007, for which COR1 (A+B) and COR1 (B) observations, respectively, could not be used due to the low contrast of the CME signatures. From Figures 2–4 it is obvious that the CMEs appear differently from different perspectives. The appearance and contrast of a CME as observed in white light depends on the line-of-sight integration of the Thomson scattered light with respect to the vantage point of the observer (Thompson et al. 1998; Plunkett et al. 1998; Vourlidas & Howard 2006). To derive the kinematics of the CME, ‘traditional’ leading edge measurements were applied. From running difference images distinct features identifiable in all three spacecraft and located along the leading edge of the CME were chosen and manually tracked in time as the CME propagated outward.

As described in Section 2, to calculate the heliospheric coordinates of the CME source region we compare two pairs of kinematics, namely LASCO/STEREO-A (LA) and LASCO/STEREO-B (LB). From this we actually obtain two results for the source region longitude φ and latitude δ . In the top panels of Figures 5–10, the distance-time measurements derived from STEREO-A (squares), STEREO-B (asterisks) and LASCO (crosses) are shown for six out of eleven CME events under study. The solid lines show the modeled distances resulting from the derived heliospheric coordinates of the source region. They actually display the LASCO measurements transformed to STEREO-A and STEREO-B views by using the derived CME source location. The fact that the evolution of the modeled distances is in a quite good match with the evolution of the actual observations from STEREO-A and STEREO-B, demonstrates the accuracy of the measurements as well as the good performance of the method. In addition, the resulting de-projected radial distances for the obtained LA and LB source region location are plotted as dashed lines. The bottom panels of Figures 5–10 show the distribution of the least square sum for the comparison between modeled and measured distances separately for LA and LB, when varying the source longitude φ in the range 0° – 180° (for the Eastern or Western hemisphere) and

Table 1: Source region of the CME separately obtained from spacecraft pairs LA and LB. Columns 1 and 2 give the derived heliographic longitudes φ , and columns 3 and 4 the latitudes δ . The last two columns show for each date the separation angles between the spacecraft pairs LA and LB. •) bad COR1 observations; °) feature measured behind the leading edge.

Date	$\varphi_{\text{LA}}(^{\circ})$	$\varphi_{\text{LB}}(^{\circ})$	$\delta_{\text{LA}}(^{\circ})$	$\delta_{\text{LB}}(^{\circ})$	$\sphericalangle\text{LA} (^{\circ})$	$\sphericalangle\text{LB} (^{\circ})$
2007-May-09	E116	E116	S08	S05	4.8	2.3
2007-May-15	E46	E50	N02	N01	5.3	2.7
2007-Jun-22	E115	E122	S14	S23	8.9	5.4
2007-Oct-08•	W70	W56	N01	N01	18.6	16.5
2007-Nov-16	W123	W117	S04	S16	20.3	20.1
2007-Dec-04°	W62	W63	N27	N13	20.7	21.4
2007-Dec-16•	E144	E152	S15	S10	20.9	22.1
2007-Dec-31	E86	E98	S15	S15	21.2	22.8
2008-Jan-02	E64	E63	N03	N01	21.2	22.9
2008-Jan-22	E104	E122	S76	S30	21.5	23.4
2008-Mar-25	E76	E89	S10	S10	23.4	23.7

a fixed (best) value of the source latitude δ . The arrows mark the minima of the distributions, i.e. the best estimation of φ from LA and LB observations. Note that for the longitude ranges $\sim 0^{\circ}$ – 20° and $\sim 160^{\circ}$ – 180° a sudden drop occurs which would meet the minimum criterion. However, these are false minima due to mathematical effects when the source region and spacecraft are close to line-of-sight.

The derived CME source location (φ , δ) is used to correct for projection effects and to obtain the ‘true’, i.e. de-projected kinematics (see Equations 1–6). The locations of the source regions obtained from LA and LB coincide mostly to within $\lesssim 10^{\circ}$ in longitude and latitude (except January 22, 2008 with difference for δ of $\sim 46^{\circ}$; cf. Table 1). For five out of eleven events the deviations between the de-projected velocities derived from LA and the de-projected velocities derived from LB are $\lesssim 1\%$ and for three events $\lesssim 5\%$ (June 22, 2007; October 8, 2007, and November 16, 2007). For another three events we found differences between LA and LB in their de-projected velocities of $\sim 10\%$ (May 15, 2007; December 16, 2007; January 22, 2008).

In Table 1 we summarize the obtained CME source region locations, derived separately from the spacecraft pairs LA and LB, together with the spacecraft position of STEREO-A and STEREO-B with respect to Earth. Table 2 contains the observed POS velocity applying a linear fit to distance measurements $R > 3R_{\odot}$ from each satellite and the derived de-projected velocity.

Inspecting the angle θ between the spacecraft line-of-sight and the CME source region on the Sun (Table 2), the true CME velocity may be directly revealed from those spacecraft where $\theta \sim 90^{\circ}$. This can be compared to the calculated de-projected speeds as a quality check for the triangulation method. We have to emphasize that this comparison is not fully independent since the

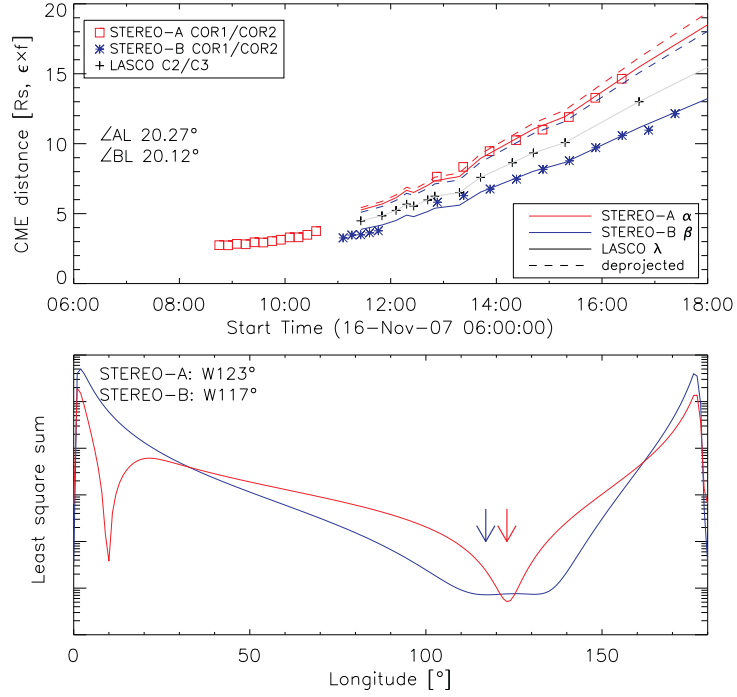


Figure 5: *Top*: Kinematics of the November 16, 2007 CME event derived from observations of different spacecraft. Red squares are for STEREO-A, blue asterisks for STEREO-B and black crosses for LASCO. Solid lines are the modeled distances for STEREO-A view (red), STEREO-B view (blue) and the reference system LASCO (gray). The red and blue dashed lines show the resulting de-projected distances separately derived from LASCO/STEREO-A and LASCO/STEREO-B comparison. The separation angle between the STEREO spacecraft with respect to LASCO is labeled ($\angle AL$, $\angle BL$). *Bottom*: Resulting distribution of least square sum as a function of the CME source region longitude φ and a fixed (best) value of the source latitude δ . The minimum is indicated by a red arrow for LASCO/STEREO-A and blue arrow for LASCO/STEREO-B.

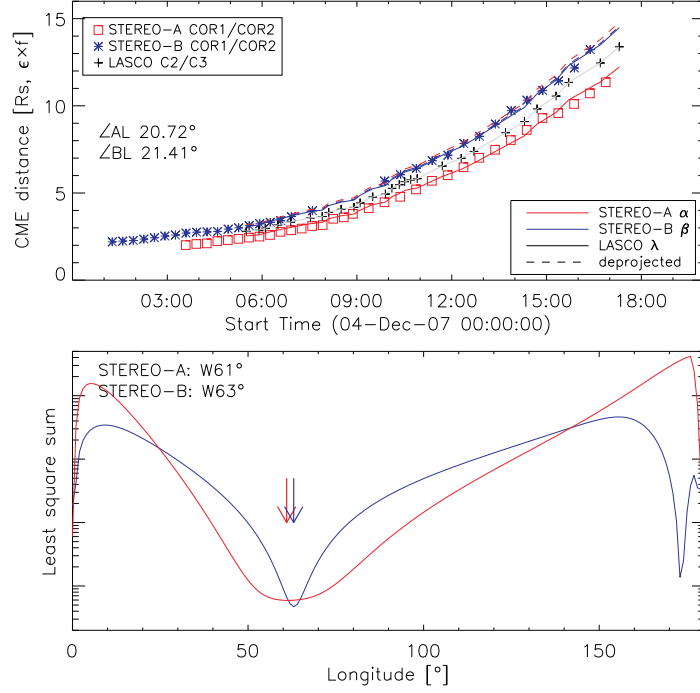


Figure 6: Same as Figure 5 but for the December 4, 2007 CME event.

Table 2: Columns 1–3 give for each spacecraft the angle (θ) between the spacecraft line-of-sight and the CME source location on the Sun (θ_L is the average between φ_{LA} and φ_{LB} ; cf. Table 1). Columns 4–6 give the POS velocity (km s^{-1}) measured from STEREO-A, STEREO-B, and LASCO observations. Columns 7 and 8 show the de-projected velocity separately obtained from spacecraft pairs LA and LB according to the derived CME source location (cf. Table 1). •) bad COR1 observations; °) feature measured behind the leading edge.

Date	θ_A	θ_B	θ_L	$v_{A_{pos}}$	$v_{B_{pos}}$	$v_{L_{pos}}$	$v_{LA_{dep}}$	$v_{LB_{dep}}$
2007-May-09	121	114	116	232	246	239	276	276
2007-May-15	51	47	48	362	325	356	456	433
2007-Jun-22	124	117	119	292	320	322	375	405
2007-Oct-08•	51	72	63	139	222	188	194	215
2007-Nov-16	103	137	120	375	275	329	418	388
2007-Dec-04°	41	84	62	178	194	192	216	214
2007-Dec-16•	165	130	148	157	225	173	322	415
2007-Dec-31	107	75	92	700	768	934	991	1013
2008-Jan-02	85	40	64	753	461	698	736	740
2008-Jan-22	125	99	113	251	341	274	375	439
2008-Mar-25	99	65	83	1109	1010	1088	1100	1090

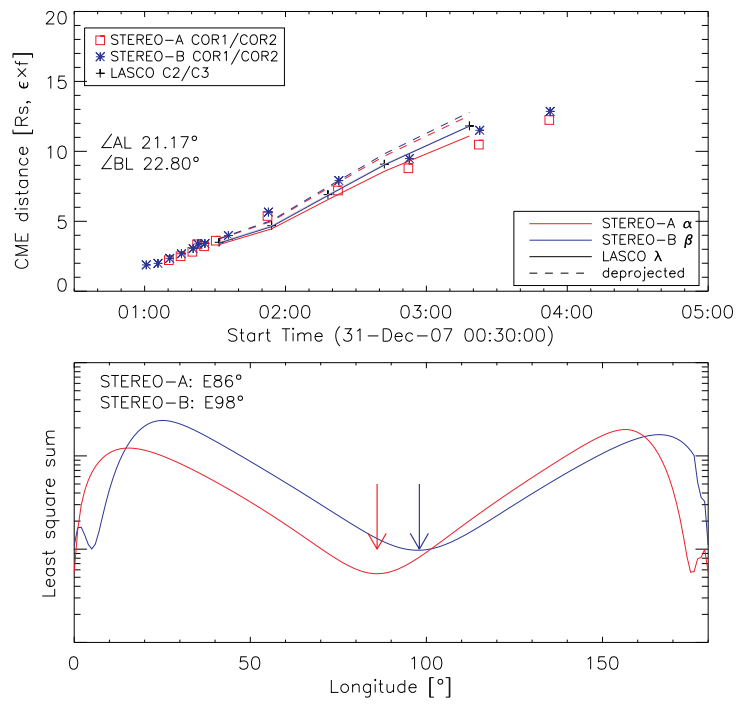


Figure 7: Same as Figure 5 but for the December 31, 2007 CME event.

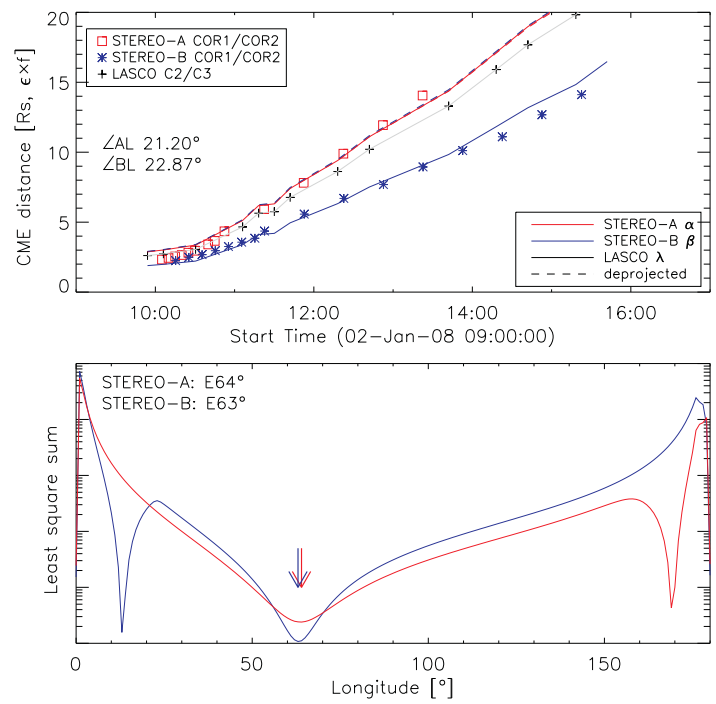


Figure 8: Same as Figure 5 but for the January 2, 2008 CME event.

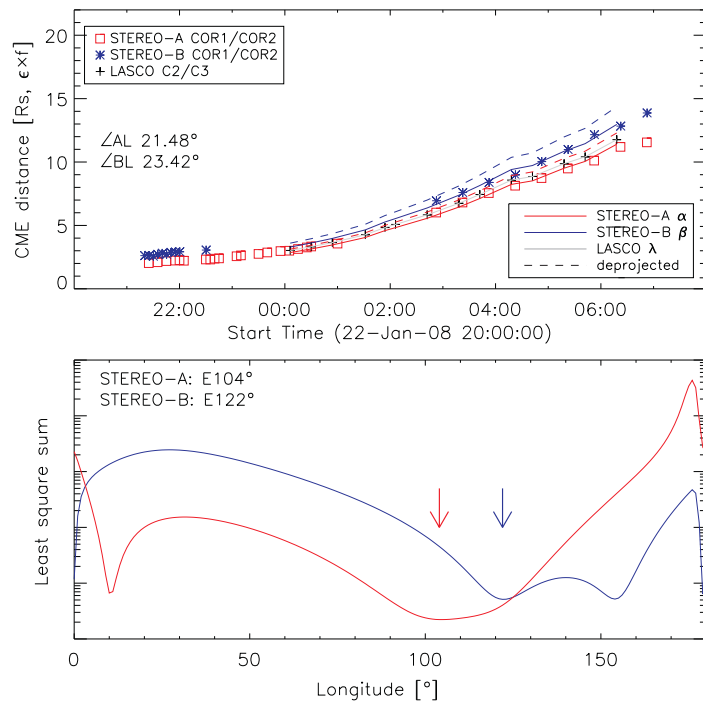


Figure 9: Same as Figure 5 but for the January 22, 2008 CME event.

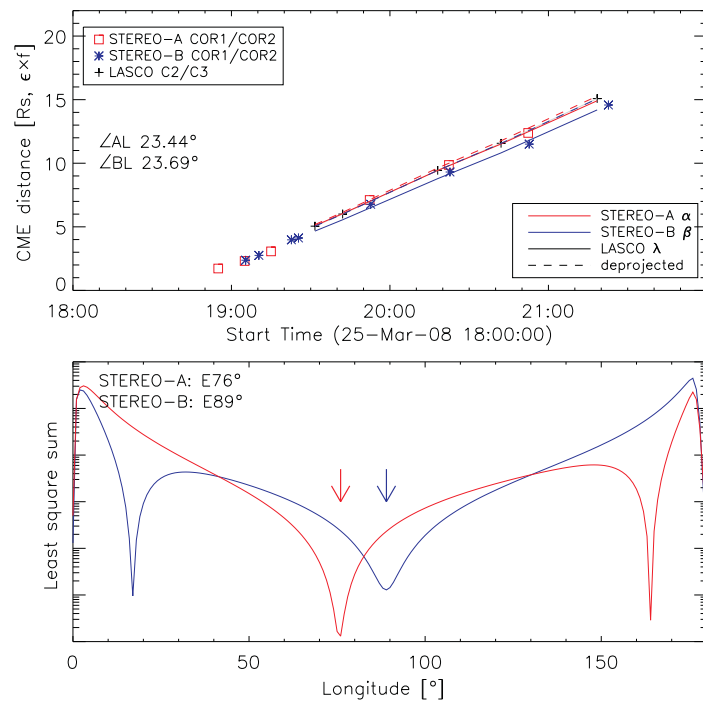


Figure 10: Same as Figure 5 but for the March 25, 2008 CME event.

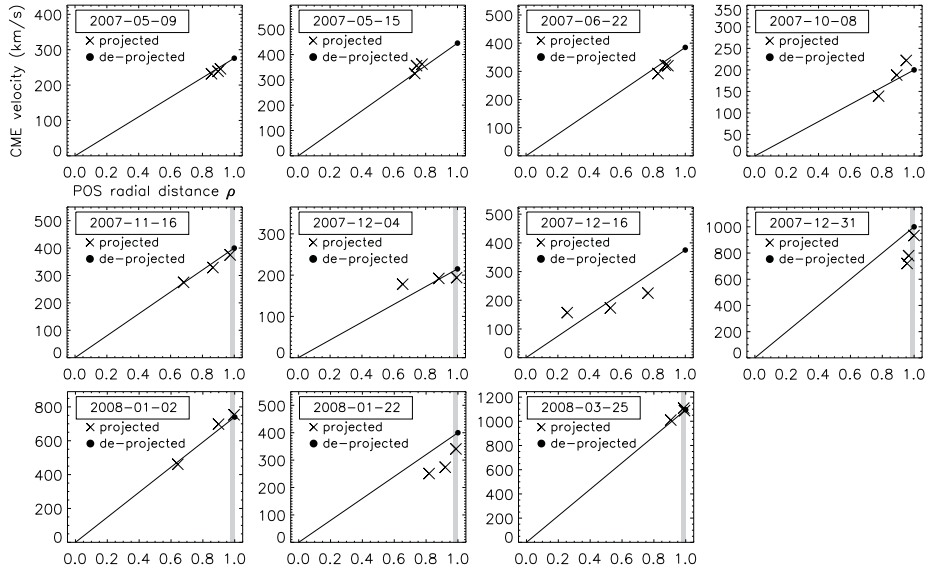


Figure 11: Relation between projected CME speed from STEREO-A, STEREO-B, and LASCO observations and the derived plane-of-sky (POS) radial distance $\rho = \sin(\theta)$ from the solar disk center. Crosses indicate the projected CME speed, filled circles the de-projected speed for each event (averaged between de-projected speeds from LA and LB). The solid line between de-projected speed at $\rho=1$ and $\rho=0$ assumes that the observed CME speed is a pure projection effect of radial expansion.

angles on which it is based are derived from the triangulation method. Table 2 shows that the projected speed from a spacecraft which observes the CME close under an angle of 90° is for most events comparable to the calculated de-projected speed. The comparison is graphically displayed in Figure 11 where the POS radial distance from the solar disk center, given as $\rho = \sin(\theta)$, is plotted against the projected velocity observed from each spacecraft. Assuming that 1) the observed CME speed is not affected by expansion, 2) the CME is radially propagating, 3) the triangulation method works properly, we expect that measured velocities are located along the connection line between $\rho = 0$ and the calculated de-projected speed at $\rho = 1$. A reasonable agreement is obtained for most of the events. In two cases (December 31, 2007, and January 22, 2008) large deviations are derived. This may be due to bad distance measurements of the CME, i.e. we can not clearly distinguish the same structural CME element in all three instruments (data scatter for the December 31, 2007 event; bad tracking for the January 22, 2008 event). The results from these events may be considered to be very low quality. For an empirical relation between CME speed and CME location covering the effects of radial and lateral expansion, we refer to Vršnak et al. (2007).

Table 3: Associated on-disk flare activity for front-sided CME events. The CME source region positions are derived from LASCO/STEREO-A (LA) and LASCO/STEREO-B (LB) observations (Table 1). For the flare activity, the GOES X-ray flare classification, its onset time, and location is listed (source: http://www.lmsal.com/solarsoft/latest_events_archive.html).

Date	LA (°)	LB (°)	GOES class	Time (UT)	Location (°)
2007-May-15	N02E46	N01E50	C1.0/B1.7	15:27/16:57	N00E52/E47
2007-Oct-08	N01W70	N01W56	A6.5	13:09	S05W25
2007-Dec-04	N27W62	N13W63	no flare rep.	—	—
2007-Dec-31	S15E86	S15E98	C8.3	00:37	S08E81
2008-Jan-02	N03E64	N01E63	C1.3	07:55	S07E75
2008-Mar-25	S10E76	S10E89	M1.7	18:36	S10E82

For a further test of our method, we checked in case of front-sided CMEs for associated flare activity. From this we found that most of the determined CME source regions are close to the observed flare regions (see Table 3). Exceptions are the events October 8, 2007 and December 4, 2007. For the October 8, 2007 only a low flaring activity in clear distance of more than 30° longitude to the derived CME source region could be associated. For the December 4, 2007 no activity at all was observed on the disk. In addition, some of our events could be compared with results derived by other authors. Thernisien et al. (2007) derived for several STEREO events the longitude and latitude by applying a flux rope forward modeling technique (Thernisien et al. 2006). Their resulting source longitudes and latitudes for events which are also in our data set, reveal a difference of $\lesssim 10^\circ$ (November 16, 2007; December 4, 2007; December 16, 2007; December 31, 2007; January 2, 2008; March 25, 2008). Results by Liewer et al. (2008) applying a 3D stereoscopy tie-point method (Liewer et al. 2006) could be compared to four events from our study (November, 16, 2007; December 31, 2007; January 2, 2008; March 25, 2008) and are found to be in good agreement of $\lesssim 10^\circ$, with exception of the November 16, 2007 event where a difference of $\sim 40^\circ$ in longitude is found. The event from November 16, 2007 was also studied by Howard & Tappin (2008) applying a geometrical analysis from which the longitude $W112^\circ$ is derived which differs from the results by Thernisien et al. (2007) with $\sim 20^\circ$ ($W132^\circ$) and by Liewer et al. (2008) with $\sim 45^\circ$ ($W159^\circ$). For the May 15, 2007 CME quite different results for the kinematics ($v \approx 169 \text{ km s}^{-1}$) and location (N14E70) are obtained by Mierla et al. (2008) who measured not the leading edge of the CME but a particular part inside the CME structure.

4 Discussion and Conclusion

To study the importance of projection effects we applied traditional CME measurements to a straight-forward triangulation method. Using CME observations from two vantage points, the method is able to determine the source region location of the CME on the solar surface (heliospheric longitude and latitude),

which is then used to correct for projection effects. With this the propagation direction and ‘true’ speed of a CME can be obtained in a simple way. However, we would like to emphasize that this kind of triangulation method relies on the assumption that we can distinguish the same structural CME element in all three instruments, which might be difficult for optically thin features like CMEs, in particular for CMEs propagating close to the line-of-sight. Thus, using observational data from STEREO we can improve the situation regarding projection effects, but cannot solve the problem completely.

With our method we transformed SOHO-LASCO distance-time measurements to STEREO-A and STEREO-B view and found a similar evolution as the distance-time measurements derived from actual STEREO-A and STEREO-B observations. This demonstrates that the method performs well. It also shows that by performing traditional leading edge measurements, features can be tracked from different vantage points with a sufficient accuracy, although the CME leading edge is extended. The modeled and measured distances from the three vantage points show a good match during the entire CME propagation up to a distance of $\sim 20R_{\odot}$, which provides evidence that CMEs expand in a self-similar manner with respect to their 3D structure (e.g. Low 1982; Maričić et al. 2004).

Comparing different methods (cf. Thernisien et al. 2007; Howard & Tappin 2008; Mierla et al. 2008; Liewer et al. 2008, this study) typical differences in the source region location are found in the range of 10° and shows the present range of accuracy. By applying traditional CME measurements we face well known limitations as some cases showed (low consistence between LA and LB results). The closer one of the spacecraft is to the line-of-sight of the CME propagation direction, the larger are the uncertainties. Furthermore, the assumption of the radial outward motion of the CME might be unjustified for some cases. This would also increase the error for the method.

In our study, we found for front-sided events and associated flare activity locations, that the source region location of fast CMEs is closer to the flare site than for slow CME events. A recent study by Yashiro et al. (2008) based on LASCO data derived that the most frequent flare site is at the center of the CME span for X-class flares while for C-class flares it is widely spread to the outside of the CME span. Thus, the presumption that the CME source region is the same as the associated flare might not be true, as pointed out by Howard et al. (2008b). The determination of the source region of a CME on the solar surface is important considering flare-CME relation aspects (e.g. Temmer et al. 2008). In addition, the location of the CME source on the solar surface is important for studies on coronal waves (e.g. Veronig et al. 2008).

Due to the absence of 3D data, several methods have been developed to correct 2D CME data for projection, which might be useful to cross-check the results derived from 3D data based methods. To derive projection effects of CMEs, cone-models are used (e.g. Cremades & Bothmer 2004; Michalek et al. 2007; Pohjolainen et al. 2007). The empirical relation between the radial POS velocity and the lateral expansion velocity of the CME is especially applicable to CMEs propagating close to the line-of-sight (Schwenn et al. 2005). Simi-

lar, the ratio between the shortest and the longest distance of the CME front as seen from the solar center might be used as indicator for forecasting CME geoeffectiveness (Moon et al. 2005; Kim et al. 2008).

The ability of STEREO to map CMEs in 3D is restricted in time by the angular separation of the two spacecraft. Thus, future CME studies will be again carried out by single coronagraph observations. Therefore it is important to improve the interpretation of ‘non 3D’ data on the basis of STEREO and LASCO results in order to gain more knowledge on how 3D features of CMEs are observed in the 2D POS coronagraphic images. With our triangulation method we could quantify and correct projection effects in the POS measurements without the need of modeling the 3D shape of CMEs (Aschwanden et al. 2008). For a quick estimation of the source region, directivity and first approximation to correct for projection effects we obtained good results which could be successfully compared to other, more sophisticated methods which are under development.

Acknowledgments

M.T. is funded by the Austrian Academy of Sciences within the Austrian Programme for Advanced Research and Technology (APART 11262). A.V. acknowledges the Austrian Fonds zur Förderung der wissenschaftlichen Forschung (FWF grant P20867-N16). The European Community’s Seventh Framework Programme (FP7/2007-2013) under grant agreement no.218816 (SOTERIA) is acknowledged. We thank the referee for valuable suggestions which helped to improve the paper.

References

- Alexander, D., Richardson, I. G., & Zurbuchen, T. H. 2006, *Space Science Reviews*, 123, 3
- Aschwanden, M. J., Burlaga, L. F., Kaiser, M. L., et al. 2008, *Space Science Reviews*, 136, 565
- Bothmer, V. 2006, *The Solar Atmosphere and Space Weather*, ed. P. Blondel & J. Mason (Springer, Berlin)
- Brueckner, G. E., Howard, R. A., Koomen, M. J., et al. 1995, *Sol. Phys.*, 162, 357
- Burkepile, J. T., Hundhausen, A. J., Stanger, A. L., St. Cyr, O. C., & Seiden, J. A. 2004, *Journal of Geophysical Research (Space Physics)*, 109, 3103
- Ciaravella, A., Raymond, J. C., & Kahler, S. W. 2006, *ApJ*, 652, 774
- Cremades, H. & Bothmer, V. 2004, *A&A*, 422, 307

- Forbes, T. G., Linker, J. A., Chen, J., et al. 2006, *Space Science Reviews*, 123, 251
- Gopalswamy, N., Lara, A., Lepping, R. P., et al. 2000, *Geophys. Res. Lett.*, 27, 145
- Gopalswamy, N., Lara, A., Yashiro, S., Kaiser, M. L., & Howard, R. A. 2001, *J. Geophys. Res.*, 106, 29207
- Gosling, J. T., Hildner, E., MacQueen, R. M., et al. 1974, *J. Geophys. Res.*, 79, 4581
- Howard, R. A., Moses, J. D., Vourlidas, A., et al. 2008a, *Space Science Reviews*, 136, 67
- Howard, R. A., Sheeley, Jr., N. R., Michels, D. J., & Koomen, M. J. 1985, *J. Geophys. Res.*, 90, 8173
- Howard, T. A., Nandy, D., & Koepke, A. C. 2008b, *Journal of Geophysical Research (Space Physics)*, 113, 1104
- Howard, T. A. & Tappin, S. J. 2008, *Sol. Phys.*, 252, 373
- Howard, T. A., Webb, D. F., Tappin, S. J., Mizuno, D. R., & Johnston, J. C. 2006, *Journal of Geophysical Research (Space Physics)*, 111, 4105
- Hudson, H. S., Bougeret, J.-L., & Burkepile, J. 2006, *Space Science Reviews*, 123, 13
- Hundhausen, A. J. 1993, *J. Geophys. Res.*, 98, 13177
- Kaiser, M. L., Kucera, T. A., Davila, J. M., et al. 2008, *Space Science Reviews*, 136, 5
- Kim, R.-S., Cho, K.-S., Kim, K.-H., et al. 2008, *ApJ*, 677, 1378
- Kunow, H., Crooker, N. U., Linker, J. A., Schwenn, R., & von Steiger, R., eds. 2007, *Coronal Mass Ejections*, ed. H. Kunow, N. U. Crooker, J. A. Linker, R. Schwenn, & R. von Steiger (Springer, Berlin)
- Leblanc, Y., Dulk, G. A., Vourlidas, A., & Bougeret, J.-L. 2001, *J. Geophys. Res.*, 106, 25301
- Liewer, P. C., Dejong, E. M., Hall, J. R., et al. 2008, *AGU Fall Meeting Abstracts*, B1556+
- Liewer, P. C., Dejong, E. M., Hall, J. R., et al. 2006, *AGU Fall Meeting Abstracts*, A1472+
- Low, B. C. 1982, *ApJ*, 254, 796

- Maričić, D., Vršnak, B., Stanger, A. L., & Veronig, A. 2004, *Sol. Phys.*, 225, 337
- Michalek, G., Gopalswamy, N., & Yashiro, S. 2003, *ApJ*, 584, 472
- Michalek, G., Gopalswamy, N., & Yashiro, S. 2007, *Sol. Phys.*, 246, 399
- Mierla, M., Davila, J., Thompson, W., et al. 2008, *Sol. Phys.*, 252, 385
- Moon, Y.-J., Cho, K.-S., Dryer, M., et al. 2005, *ApJ*, 624, 414
- Pizzo, V. J. & Biesecker, D. A. 2004, *Geophys. Res. Lett.*, 31, 21802
- Plunkett, S. P., Thompson, B. J., Howard, R. A., et al. 1998, *Geophys. Res. Lett.*, 25, 2477
- Pohjolainen, S., van Driel-Gesztelyi, L., Culhane, J. L., Manoharan, P. K., & Elliott, H. A. 2007, *Sol. Phys.*, 244, 167
- Riley, P. & Crooker, N. U. 2004, *ApJ*, 600, 1035
- Schwenn, R., dal Lago, A., Huttunen, E., & Gonzalez, W. D. 2005, *Annales Geophysicae*, 23, 1033
- Sheeley, N. R., Walters, J. H., Wang, Y.-M., & Howard, R. A. 1999, *J. Geophys. Res.*, 104, 24739
- St. Cyr, O. C., Plunkett, S. P., Michels, D. J., et al. 2000, *J. Geophys. Res.*, 105, 18169
- Temmer, M., Veronig, A. M., Vršnak, B., et al. 2008, *ApJ*, 673, L95
- Thernisien, A. F., Howard, R. A., & Vourlidas, A. 2007, *AGU Fall Meeting Abstracts*, A778+
- Thernisien, A. F. R., Howard, R. A., & Vourlidas, A. 2006, *ApJ*, 652, 763
- Thompson, B. J., Plunkett, S. P., Gurman, J. B., et al. 1998, *Geophys. Res. Lett.*, 25, 2465
- Thompson, W. T. 2006, *A&A*, 449, 791
- Veronig, A. M., Temmer, M., & Vršnak, B. 2008, *ApJ*, 681, L113
- Vourlidas, A. & Howard, R. A. 2006, *ApJ*, 642, 1216
- Vršnak, B., Ruždjak, D., Sudar, D., & Gopalswamy, N. 2004, *A&A*, 423, 717
- Vršnak, B., Sudar, D., Ruždjak, D., & Žic, T. 2007, *A&A*, 469, 339
- Vršnak, B. & Žic, T. 2007, *A&A*, 472, 937
- Webb, D. F., Cliver, E. W., Crooker, N. U., Cry, O. C. S., & Thompson, B. J. 2000, *J. Geophys. Res.*, 105, 7491

- Webb, D. F. & Howard, R. A. 1994, *J. Geophys. Res.*, 99, 4201
- Webb, D. F., Mizuno, D. R., Buffington, A., et al. 2006, *Journal of Geophysical Research (Space Physics)*, 111, 12101
- Xue, X. H., Wang, C. B., & Dou, X. K. 2005, *Journal of Geophysical Research (Space Physics)*, 110, 8103
- Yashiro, S., Michalek, G., Akiyama, S., Gopalswamy, N., & Howard, R. A. 2008, *ApJ*, 673, 1174
- Zhang, J., Dere, K. P., Howard, R. A., & Bothmer, V. 2003, *ApJ*, 582, 520